European Conference on Computational Fluid Dynamics
ECCOMAS CFD 2006
P. Wesseling, E. Oñate and J. Périaux (Eds)

MODEL AND FULL-SCALE FREE-SURFACE VISCOUS FLOWS AROUND FULLY-APPENDED SHIPS

M. Visonneau*, P. Queutey* and G.B. Deng*

*Fluid Mechanics Laboratory - UMR6598 - CFD department
Ecole Centrale de Nantes
BP 92101
44321 Nantes, France
e-mail: Michel.Visonneau@ec-nantes.fr

Key words: Appended hull, hexahedral unstructured grid, uncertainty estimation, vortical flow

Abstract. *Two appended hull configurations have been simulated using all hexahedral unstructured grids. Numerical uncertainty is assessed with grid refinement. Influence of turbulence model and wall function approach have been investigated. Scale effect is also studied for one configuration. Numerical results are validated both with measurement data and with computational results using structured grid when possible.*

1 INTRODUCTION

In spite of considerable progresses made during the last decade both in hardware and software development, the accurate prediction of turbulent flow around appended hull remains a challenging task. In addition to appropriate turbulence model, the success of a numerical simulation depends on the quality of the body-fitted grid employed for the computation. For a simple geometry, a good quality block-structured grid can be generated with available grid generation software, at least near the solid wall. However, for more complex geometries such as a hull with appendages, the generation of a good quality block-structured grid is not a trivial task and may take weeks of human time. Although unstructured tetrahedral grid can be easily generated for such complex geometry, most of the flow solvers employed in engineering applications such as those based on second order finite volume method are unable to give accurate numerical solution with such grids. Another efficient way to handle complex geometries is to use a Cartesian grid associated with the immersed boundary method. Although reasonable prediction for inviscid flow can be obtained, the accuracy of an immersed boundary method for turbulent flow especially at high Reynolds number remains to be demonstrated. Based on the Cartesian grid approach, recent grid generation softwares such as HARPOON and HEXPRESS offer the possibility to capture the viscous layer with body-fitted grid while maintaining the flexibility of the unstructured grid and the accuracy of hexahedral element. However, compared with conventional block-structured body-fitted grid, the viscous layer near the body surface is usually not well captured. In addition, it contains non-conformal elements in finite element sense. Furthermore, like all unstructured grid generators, the grid density in the computational domain is not well controlled. Hence, the accuracy of a numerical computation using such kind of grid needs to be evaluated. The present study is devoted

to this issue. Effect of turbulence modelization will also be addressed. For a bare hull configuration, the most challenging task in turbulence modelization is the modelization of vortical flows due to the bilge vortex developed in the aft-part of the ship. A correct prediction of this phenomenon requires advanced turbulence models such as nonlinear model or even Reynolds stress transport model, associated sometimes with empirical corrections. Additional vortical structures may appear when appendages are added, making the task of turbulence modelization even more challenging. The sensitivity to turbulence model as well as to the validation of wall function approach will be investigated.

2 THE NUMERICS

Computations are performed with the ISIS-CFD flow solver developed by EMN (Equipe Modélisation Numérique, i.e. CFD Department of the Fluid Mechanics Laboratory). Turbulent flow is simulated by solving the incompressible unsteady Reynolds-averaged Navier-Stokes equations (RANSE). The solver is based on the finite volume method to build the spatial discretization of the transport equations. The face-based method is generalized to two-dimensional, rotationally-symmetric, or three-dimensional unstructured meshes for which non-overlapping control volumes are bounded by an arbitrary number of constitutive faces. The velocity field is obtained from the momentum conservation equations and the pressure field is extracted from the mass conservation constraint, or continuity equation, transformed into a pressure-equation. In the case of turbulent flows, additional transport equations for modeled variables are discretized and solved using the same principles. Free-surface flow is simulated with a multi-phase flow approach. Incompressible and non-miscible flow phases are modelized through the use of conservation equations for each volume fraction of phase/fluid. Several turbulence models ranging from one-equation model to Reynolds stress transport model are implemented in ISIS-CFD. Most of the classical linear eddy-viscosity based closures like the Spalart-Allmaras one-equation model [1], the two-equation $k-\omega$ SST model by Menter [2], for instance are implemented. Two more sophisticated turbulence closures are also implemented in the ISIS-CFD solver, an explicit algebraic stress model (EASM) [3] and a Reynolds stress transport model [4].

3 THE FRIGATE "LE COMMANDANT RIVIERE"

3.1 Description

The first ship studied in this article is a frigate called "Le Commandant Rivière". Experimental studies were performed both in water channel and in towing tank in the Bassin d'Essais des Carènes (BEC) [5]. A 1/14.725 model is employed in the experimental study with a L_{PP} length of 6.655 meter, a breadth of 0.782 meter, and a fixed draught of 0.228 meter. The water channel measurement have been performed with three different incoming velocities V=1.3 m/s, 6.0 m/s and 11.5 m/s, giving a Reynolds number of 8.7x106, 4.0x107 and 7.3x107 respectively. Velocity field at the propeller plane has been measured both for the bare hull and the appended hull configurations. The appendages of the frigate "Le Commandant Rivière" are composed of sonar bulb, rudder, shafts and struts. In a towing tank, an experimental study has been performed only with the appended hull configuration with and without propeller for three different velocities V=1.3 m/s, 2.0 m/s and 2.7 m/s, giving a Reynolds number of 8.7x106, 1.3x107 and 1.8x107 respectively.

In addition to the propeller plane, velocity field was measured at one plane before and another plane behind the propeller for the case V=1.3 m/s. Unfortunately, resistance results are not available for both configurations. The present numerical study will focus mainly on the water channel configuration for the test case with Re=8.7x106. The water channel GTH ("Grand Tunnel Hydrodynamique") at Val de Reuil is 10 meter long, 2 meter wide and 1.35 meter high. The frigate model is attached to the upper channel wall. A preliminary computation taking into account the real water channel configuration shows that the channel walls have limited effect on the velocity field in the propeller plane. To save computational resources, nearly all computations presented in the present study were performed on an infinite domain with a double model without taking into account the channel wall and the free-surface. The computational domain is extended to $1.5L_{PP}$ before, $3.5L_{PP}$ behind, and about $2L_{PP}$ around the ship and a uniform flow is imposed at the outer boundary. The commercial software HEXPRESS developed by NUMECA is employed for grid generation. HEXPRESS generates an all hexahedral unstructured grid. Fig. 1(a) shows an example of surface grid generated by HEXPRESS.

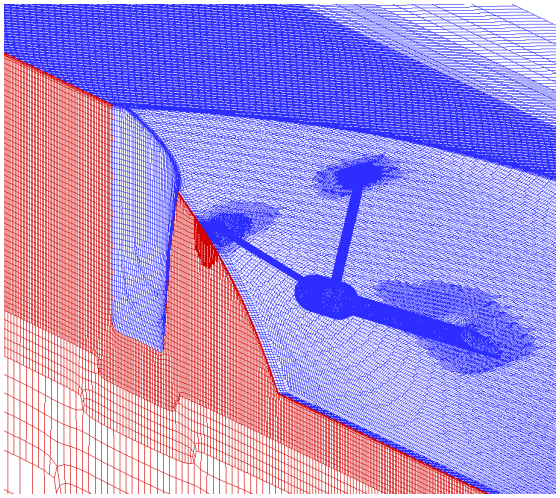

(a) Surface grid

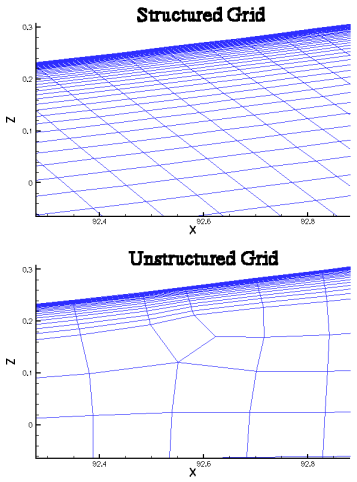

(b) Structured vs unstructured grids

Figure 1: Surface grid around the Commandant Rivière

3.2 Validation for the bare hull configuration

As mentioned above, the viscous layer near the body surface is usually not well captured with the grid generated by HEXPRESS (see Fig. 1(b)). In addition, it contains non-conformal elements in finite element sense. In order to evaluate the numerical error induced by such a grid, a first validation has been carried out with the bare hull configuration for which structured grids can be easily generated for comparison. The flow around the bare hull is first computed using a set of three structured grids. Grid dimensions as well as the predicted resistance coefficients are shown in Table 1.
The $k-\omega$ SST model is employed for the computation without using wall function. Although monotonous convergence behavior is observed for all resistance coefficients, the observed order of accuracy (8 for Cp and 0.5 for Cf) differs too much from the expected value. The last line in Table 1 gives the extrapolated value using the error estimation ap-

Case	Dimension	Cp	Cf	Ct
Grid3	$129 \times 65 \times 33$	0.000124	0.003002	0.003127
Grid2	$161 \times 81 \times 41$	0.000117	0.003019	0.003137
Grid1	$193 \times 97 \times 49$	0.000116	0.003032	0.003148
Extrap.		0.000114	0.003093	0.003207

Table 1: Resistance predicted with structured grids

Case	Dimension	Cp	Cf	Ct
Grid3	1219888	0.000113	0.002913	0.003026
Grid2	2494508	0.000102	0.002902	0.003003
Grid1	3812705	0.000108	0.002910	0.003018
Grid3L	2317144	0.000118	0.002934	0.003052

Table 2: Resistance predicted with unstructured grids

proach proposed by Stern et al. [6] by assuming that the theoretical orders of accuracy for Cp and Cf are 2 and 1, respectively, which gives an uncertainty level of 4.4% and 4.1% for Cp and Cf respectively. The choice of first order accuracy for Cf is based on a previous study for the KVLCC2M test case [7]. Compared with the ITTC 1957 friction coefficient line Cf0=0.003074, the estimated friction resistance coefficient Cf=0.003093 is only 0.6% higher. Hence the accuracy of the extrapolated resistance coefficients can be considered as appropriate. On the fine grid (Grid 1), the friction resistance is under-estimated by about 2%. This is in agreement with what we have found for the KVLCC2M test case mentioned above. This relatively high level of error with such a fine grid (about 1 million nodes) is partially due to the ill-posed boundary condition of the ω equation. With the Spalart-Allmaras model for example, this error is expected to be smaller than 0.5% with such a fine grid. Numerical accuracy for computation using unstructured grid has also been performed for the bare hull configuration using three different grids. Grid dimensions as well as the predicted resistance coefficients are given in Table 2. As the similarity between different grids can not be ensured as for the case of structured grid with systematic grid refinement, in addition, wall function approach is used, it is unlikely possible to evaluate the numerical uncertainty with the Grid Convergence Index approach. Nevertheless, the data range observed between different grids can give an indication on numerical uncertainty. For Cp, the data range is relatively high (about 10%). Compared with the extrapolated resistance coefficients obtained with structured grid, the pressure resistance is under-estimated by 1 to 10% depending on the grid. Concerning Cf, the data range is only about 0.4%, indicating that the solutions are nearly grid independent. However, compared with the extrapolated value obtained with the structured grids, it is under-estimated by about 6%. As the pressure resistance represents less than 4% of the total resistance, the total resistance is under-estimated by about 6% when using the unstructured grid. No improvement is observed with grid refinement. The error in friction resistance is too high even when uncertainty level associated with the result obtained on the structured grid is taken into account. This under-estimation is unlikely due to the use of wall function, since a computation using low Reynolds number increases the friction

resistance only by 0.7% as shown in Table 2 in the last line (comparison between Grid 3 and Grid 3L who share a common grid except for near wall cells). We believe that this relatively high level of error that can not be efficiently reduced by grid refinement is due to the way HEXPRESS generates an unstructured grid. It begins by generating a grid almost isotropic in all directions around the body. Then, the first grid cells attached to the wall are divided in the wall normal direction to build a viscous layer. Consequently, unlike a structured grid, HEXPRESS is unable to ensure a smooth transition between highly stretched wall-boundary cells and nearly isotropic volume cells as illustrated in Fig. 2. Unless the size of volume cell can be reduced as the same size of wall-boundary cells, which is virtually impossible due to limitation of computer resources for high Reynolds number flow, this default can not be cured with grid refinement. Nevertheless, error induced by such default is now well identified and quantified as about -5%, which can be considered as acceptable for engineering application. Concerning the prediction of the velocity field, the streamwise velocity component differs only by 0.5% between the coarse and the fine grid in the measurement windows in the propeller plane for the computation using structured grid. For the unstructured grid, this difference is reduced to about 0.25%. For both cases, numerical results can be considered as grid independent. However, when one compares the result obtained with the structured grid and with the unstructured grid, the difference is about 2% (Fig. 2(a)).

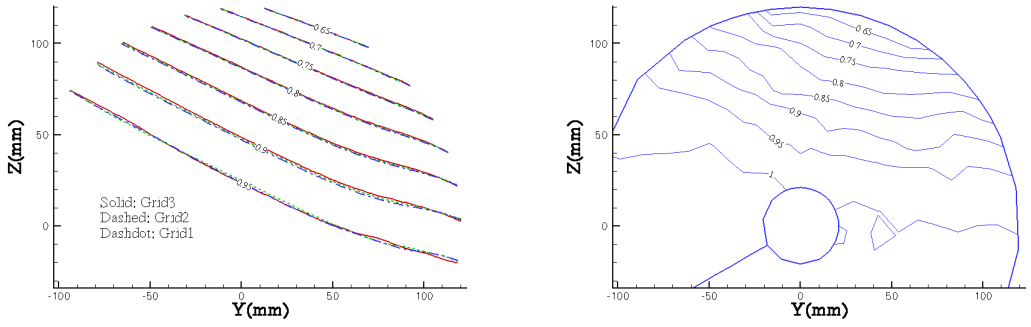

(a) Computations (b) Experiments

Figure 2: Predicted and measured streamwise velocity contours at the propeller plane for V=1.3 m/s

This difference is reduced to 1.4% when low Reynolds number model is also employed in the computation with unstructured grid. Numerical prediction obtained with the SST model agrees reasonably well compared with the measurement result shown in Fig. 2(b). The free-stream value for the U velocity differs by about 5% between computations and measurements. This is mainly due to the choice of reference velocity. In the measurement, free-stream U velocity is chosen as reference, while in the computation, inflow velocity is chosen as reference. In addition, measurement has been done in water channel, while computations are performed in infinite domain. Both the simulation and the measurement show that for the bare hull configuration, flow is quite simple. Bilge vortex does not exist. What one observed in the propeller plane is the result of the development of the boundary layer along the hull. Prediction given by the SST model can be considered as reliable for such a simple flow.

Case	Dimension	Cp	Cf	Ct
G3EL	4554531	0.000572	0.003351	0.003924
G2EL	8788858	0.000544	0.003366	0.003909
G1EL	12819606	0.000536	0.003382	0.003918
G3SL	4554531	0.000547	0.003380	0.003927
G2SL	8788858	0.000529	0.003377	0.003905
G3SW	1165843	0.000585	0.003462	0.004047
G2SW	5793493	0.000563	0.003377	0.003940

Table 3: Resistance prediction for the appended hull (E: EASM model, S: SST model, L: Low Reynolds number model, W: wall function approach)

3.3 Predictions for the appended hull configuration

As for the bare hull configuration, computations have also been performed on three different grids in order to evaluate numerical uncertainty. The ship surface including all appendages is discretized with about 125000, 200000 and 300000 grid points respectively for the coarse, medium and fine grids, while the volume grid contains about 4.5, 8.8 and 12.8 million nodes, respectively. Due to the fact that grid points can not be efficiently clustered in the wall normal direction, the unstructured grid generated by HEXPRESS contains more grid points compared to a classical body-fitted block-structured grid. In addition, the above mentioned grids are designed for computation using low Reynolds number model. Due to the high density of the surface grid, the number of grid points becomes very large. Two turbulence models have been employed, namely the $k-\omega$ SST model and the Explicit Algebraic Stress Model (EASM). A rotation correction [8] is applied in the computation using the EASM model. The first model is selected to represent linear eddy-viscosity model commonly used in engineering applications, while the second is selected because of its capability to provide improved prediction for stern flows involving vortical structure. Computations were first performed with wall function approach as for the bare hull configuration, but as explained below, low Reynolds number model is preferred in later computations in order to ensure good numerical accuracy.
Results for resistance prediction are summarized in Table 3. Computations obtained with the EASM model using low-Reynolds number model give a monotonous convergence behavior for Cp and a monotonous divergence behavior for Cf (cases G3EL, G2EL and G1EL). With an observed order of accuracy of 3.9 for Cp, it is difficult to obtain a reliable estimation for numerical uncertainty using the extrapolated value Cp=0.000523. With the error estimation approach proposed by Stern et al. [6], one obtains an extrapolated value for Cp of 0.000507 with an uncertainty level of 9%. The monotonous divergence with an observed order of accuracy of -3.7 for Cf does not imply that the result of numerical computation is highly uncertain, since the grid sets employed for the grid dependency study is not a grid set with systematic refinement due to the limitation of the grid generation software. Using three times the data range as suggested by Eça and Hoekstra [9], the uncertainty level is estimated as 3%, which can be considered as satisfactory. The same approach applied to the total resistance gives an uncertainty level of 1%, which confirms the good quality of the prediction. Compared with the bare hull configuration, the pressure resistance increases by about 5 times, while the friction and total resistances are

increased by about 17% and 30% respectively. For the KVLCC2M test case investigated in the previous study [7], it was found that the EASM model increases the prediction of the pressure resistance by about 15% compared with the SST model, resulting in an improvement for the total resistance prediction. For the present configuration, the pressure resistance increases only about 3% when the EASM model is employed. This different behavior can be explained by the fact that, for the KVLCC2M test case, influence of the bilge vortex on pressure resistance is important. As the EASM model improves the prediction of the bilge vortex, the result of pressure resistance is improved. In the present configuration, pressure resistance depends more on the modifications introduced by the appendages. Consequently, pressure resistance is less sensitive to turbulence modelization. For the friction resistance, the prediction given by the EASM model is about 1% smaller than that given by the SST model. Both models give almost the same prediction for the total resistance. The uncertainty level for the mean velocity field becomes higher than the bare hull configuration. Fig. 3 compares the streamwise velocity contours at the propeller plane predicted by the EASM model on three different grids. From the coarse to the fine grid, the difference is less than 2% in most part of the measurement windows, while from the medium grid to the fine grid, this difference is reduced to 1%.

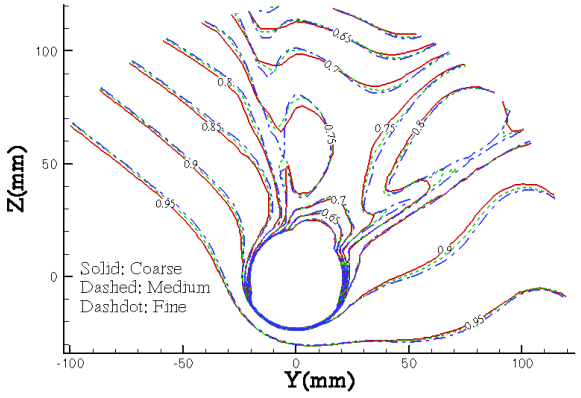

Figure 3: U velocity contours at the propeller plane predicted with three different grids with the EASM model for V=1.3 m/s

As for the bare hull configuration, computations were first performed with the SST model using wall function. Results were found to be very sensitive to grid resolution. The U velocity differs by 8% in some region of the measurement windows at the propeller plane between the coarse and the medium grid as displayed in Fig.4(a). When a low Reynolds number model is applied, the solution differs only by 1% between the two grids (Fig. 4(b)). Grids employed in both computations differ only in the near wall region. As the computations using the same approach with similar grid density give nearly grid independent solutions for the bare hull configuration, appendages are responsible for the failure of the wall function approach. However, such default can not be eliminated if low Reynolds number model is applied only to the surface of the appendages. In fact, the main reason for which wall function approach fails is the interaction between the longitudinal vortex originated from the sonar bulb and boundary layer along the hull. Low Reynolds model must be applied in the region near the vortex along the hull as well. In order

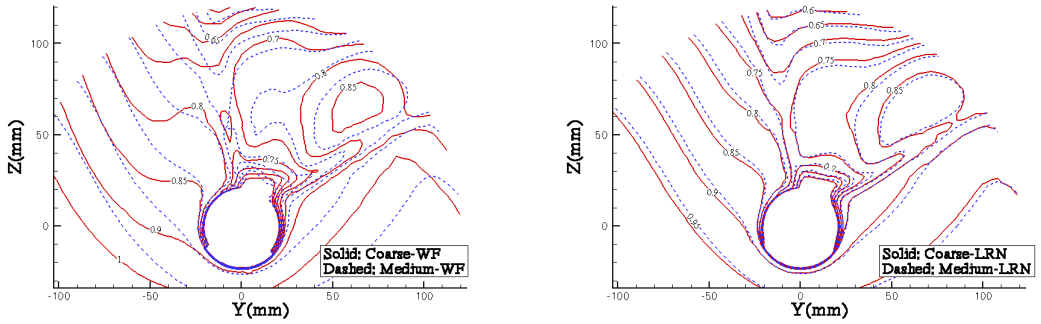

(a) Wall function (b) Low Re number

Figure 4: U velocity contours predicted by the SST model using low Reynolds number and wall function formulations

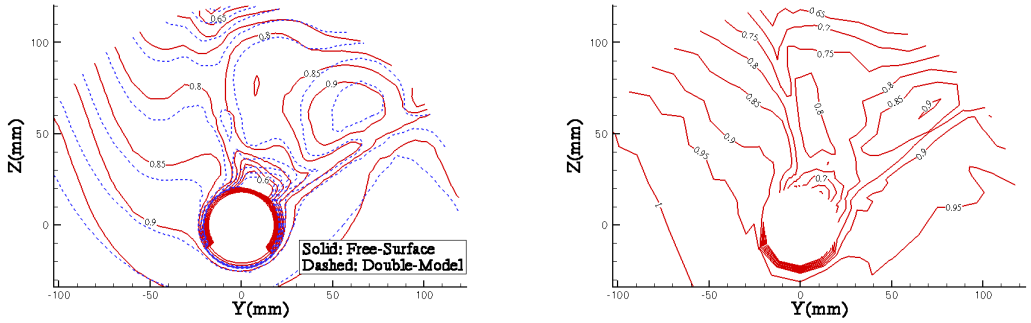

(a) Computations: Free-surface vs double-model (b) Experiments: water channel

Figure 5: Comparison between free-surface, double-model computations (SST model with wall function) and experiments in water channel (propeller plane at V=1.3 m/s)

to ensure a good numerical accuracy, wall function approach is not employed for the computation using the EASM model.

Free-surface and double-model computations are compared in Fig. 5(a). Both computations use the SST model and wall function and a similar grid density corresponding to the coarse grid mentioned above. They give similar prediction, indicating that the effect of free-surface on the velocity field is not large at this measurement plane. Measurement results for streamwise velocity contours at the propeller plane obtained in the water channel are displayed in Fig. 5(b). The measurement section is located just behind the struts. Successful prediction of the velocity field at this section depends both on a correct prediction of the boundary layer along the hull and on a correct prediction of the flow around the shaft and the struts. Since the flow does not separate around the above mentioned appendages, it is the first phenomenon that is more difficult to predict with accuracy due to the interaction of the longitudinal vortex and the boundary layer. The existence of two local maximum velocity zones behind both struts in the inner side for example, is certainly not due to the acceleration of the fluids around the struts, but the imprint of high velocity region of the upstream vortical structures. Among all the computations presented previously, only the EASM model is capable to predict correctly these two local maximum velocity regions. Further investigations reveal that the better prediction obtained with the

EASM model is mainly due to the rotation correction rather than the non-linear terms in the model.

4 THE HOPPER-DREDGER "UILENSPIEGEL"

4.1 Description

The second test case is an hopper-dredger called Uilenspiegel built by IHC HOLLAND Dredgers BV. The geometry of the dredger Uilenspiegel is more complex than the frigate. In addition to all appendages present in the previous configuration except the sonar bulb, it also contains a nozzle and a triangular base (called headbox) that supports the nozzle and the rudder. Fig. 6 shows the surface grid generated by HEXPRESS. It contains about 6 million nodes, among them about 340 000 are located on the hull. Computations have been performed at full scale ($Re = 1.03 \times 10^9$) and model scale (1:23.5, $Re = 8.27 \times 10^6$) with and without propeller. The free-surface flow is computed with a free-surface capturing approach and the propeller action is modeled by an actuator disk.

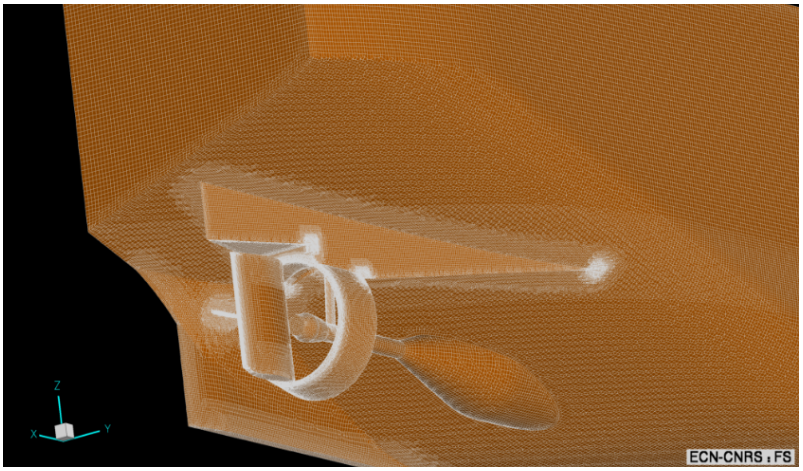

Figure 6: **Uilenspiegel**: Surface grid around the Uilenspiegel

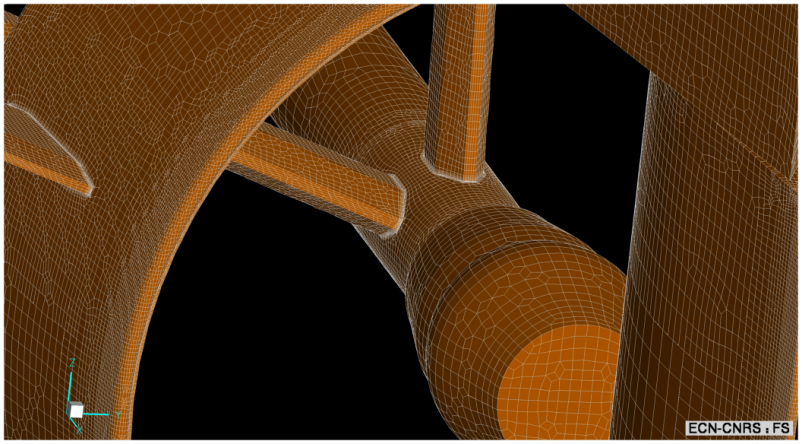

Figure 7: **Uilenspiegel**: Nozzle, V-brackets and shaft details

A magnified view to evaluate the level of representation of the discretised geometry about appendages is also given with Figure 7.

4.2 Computations

4.2.1 Free-surface

The overall wave system is illustrated with Figures 8 and 10 which provide a comparison between the full scale (**FS**) and the model scale (**MS**) conditions and no dramatic differences can be qualitatively detected.

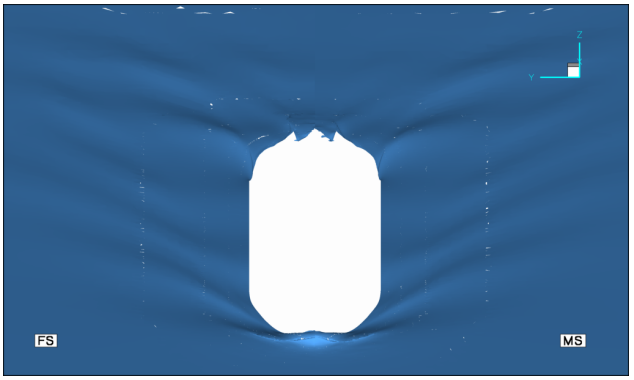

Figure 8: **Uilenspiegel**:**WOP**: 3D view comparison between the **FS** and **MS** wave system

Details about the bow wave region are presented with Figure 9 where the wave breaking is clearly visible.

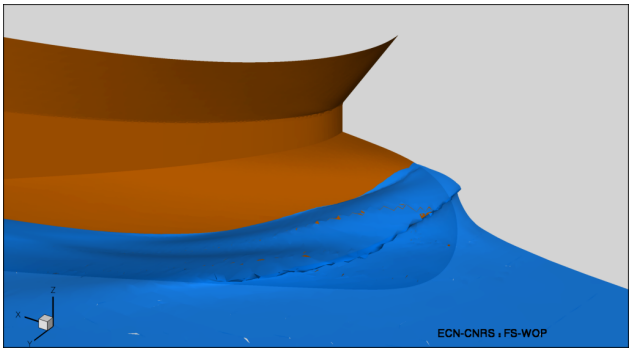

Figure 9: **Uilenspiegel**:**FS**:**WOP**: 3D side view of the breaking bow wave

4.2.2 Wall streamlines

Figures 11 show the limiting wall streamlines of model scale free-surface flows with and without propeller. Due to computational ressources limitations and for time saving, the air/water volume fraction for the simulation with propeller (**WIP**) is frozen to the field obtained without propeller (**WOP**). One can observe the strong upstream influence of the ducted propeller on the near-wall flow and the drastic reduction of separated flow regions when the propeller is working. At model scale and without propeller, one can see the print

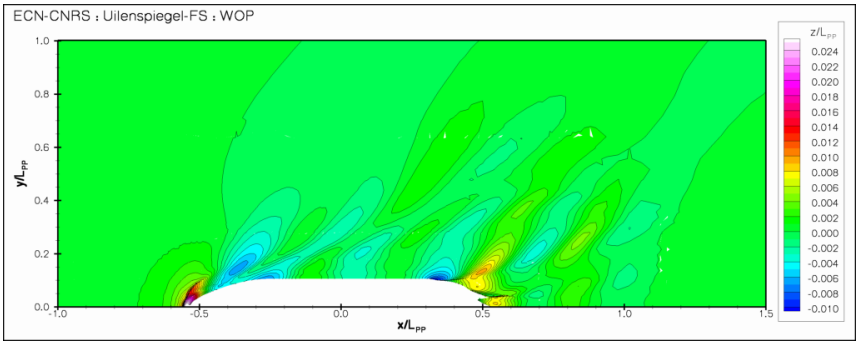

(a) **FS**

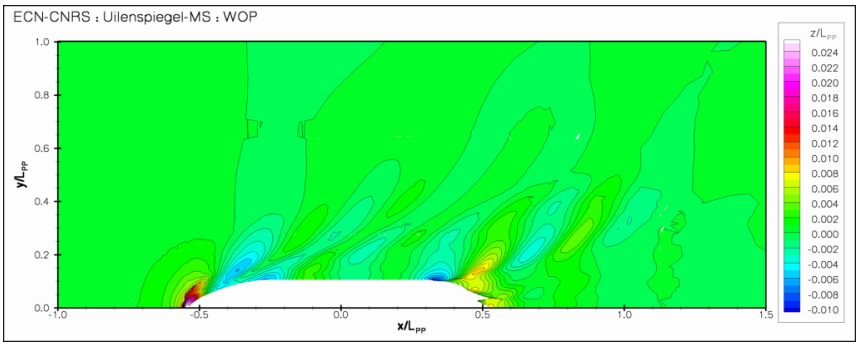

(b) **MS**

Figure 10: **Uilenspiegel**:**WOP**: Normalized wave elevations

of a very complex structure made of three longitudinal vortices visible from their focal prints near the intersection between the hull and the propeller shaft. When the propeller is activated, one longitudinal vortex disappears and the two remaining ones seem to be sucked by the propeller. One can also notice that the wall flow on the propeller shaft is strongly influenced by the propeller, as expected.

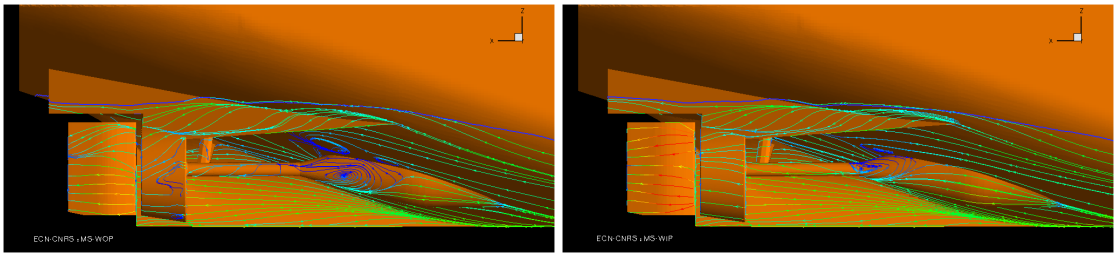

(a) **WOP** (b) **WIP**

Figure 11: **Uilenspiegel**:**MS**: Limiting wall streamlines

Figure 12 shows the limiting wall streamlines of full scale free-surface flows with and without propeller. One can observe again the strong upstream influence of the ducted propeller on the near-wall flow and the drastic reduction of separated flow regions when the propeller is operating. Compared to the computations performed at model scale (fig. 12), the Reynolds number influence appears to be very significant since, even without propeller, the three strong longitudinal vortices emanating from the neighbourhood of the intersection between the hull and the propeller shaft, have totally disappeared.

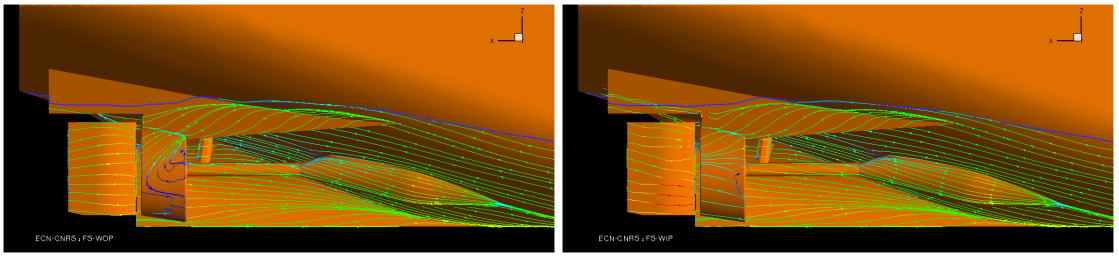

(a) **WOP** (b) **WIP**

Figure 12: **Uilenspiegel**:**FS**: Limiting wall streamlines

Case	Cp	Cf	Ct
MS:WOP	0.00359	0.00318	0.00677
MS:WIP	0.00391	0.00332	0.00723
FS:WOP	0.00361	0.00169	0.00530
FS:WIP	0.00277	0.00173	0.00449

Table 4: Resistance prediction for the Uilenspiegel (MS: model scale, FS: full scale, WOP: without propeller, WIP: with propeller)

4.2.3 Force coefficients

Resistance results are summarized in Table 4. Grid dependency study has not been performed for this test case. At model scale, unlike the previous case, the viscous resistance at model scale without propeller agrees well with the ITTC 1957 estimation (0.00318 compared with Cf0=0.00310). This may be due to the fact that the surface of appendages represents only about 1.2% of the total wetted surface. Hence, the influence of appendages on viscous resistance is limited. At full scale, the predicted viscous resistance for the case without propeller Cf=0.00169 is 10% higher than the ITTC 1957 estimation Cf0=0.00153. This is a usual observation in full scale computation. What is somewhat unexpected is that the pressure resistance is reduced at full scale when the propeller is in action, while it is increased at model scale. This behavior can be explained by the fact that aft-body flow structures are quite different in model scale and in full scale as illustrated in Fig. 11(b) and Fig. 12(b) where the predicted wall streamlines at model and full scale, respectively, are shown with the influence on the vortical structures of the suction related with the propeller effect. A multiple vortex structure is present in model scale simulation which interacts with the nozzle and the rudder, while these vortices disappear or become very weak in full scale. Experimental visualization confirms the existence of the multiple vortex structures predicted at model scale. Activation of the propeller modifies considerably those structures, resulting in the above mentioned variation in Cp.

4.2.4 Scale effects

With the following results, it is possible to carry out a study of the scale influence on the isowake distribution in the vicinity of the ducted propeller. Figures 13 to 15 show the isowake contours at model and full scale with propeller. As indicated previously, the scale effect is clearly visible on the respective boundary layer thicknesses. Figure 13 shows

again the acceleration of the flow in the region located between the propeller shaft and the hull, a phenomena which is illustrated by the wall streamlines at full scale. In Fig. 14, one can see that the vortical structure which is convected between the V-brackets at model scale has somewhat disappeared at full scale and the longitudinal velocity component seems to be more homogeneous below the propeller shaft at full scale. The same remark applies to Fig. 15.

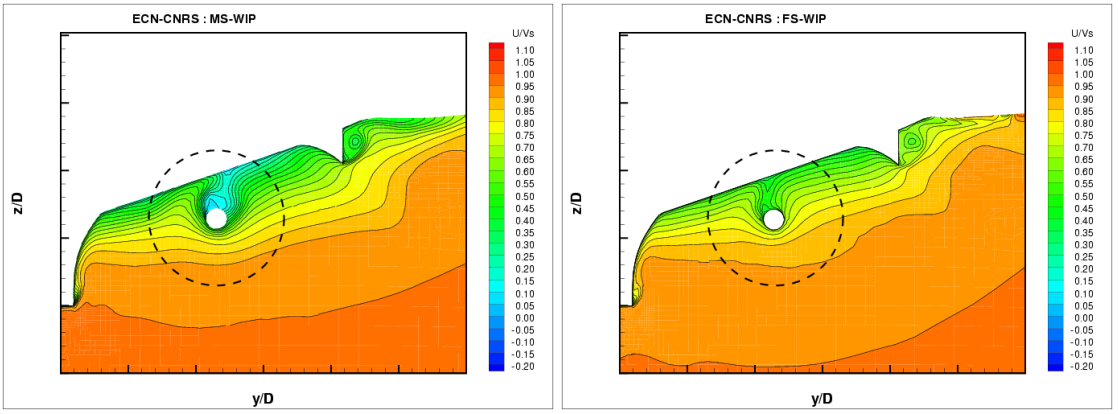

(a) **MS** (b) **FS**

Figure 13: **Uilenspiegel**:**WIP** Scale influence on the isowakes at station 1

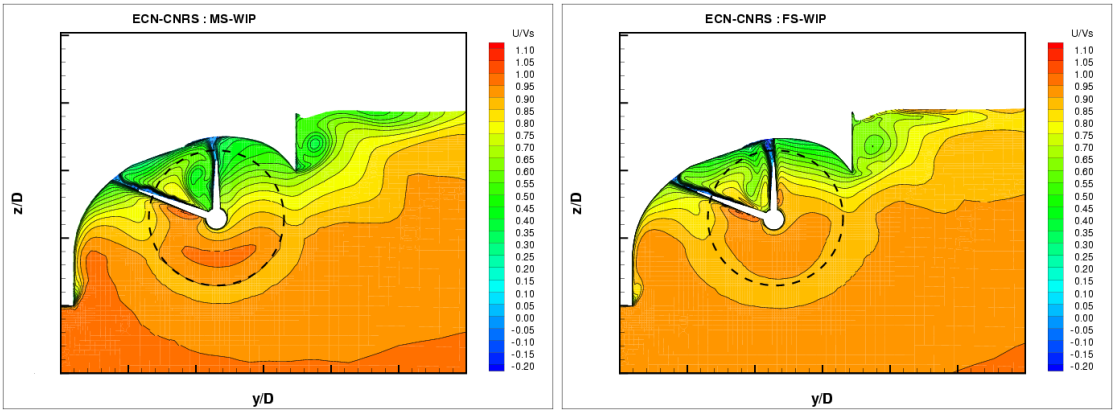

(a) **MS** (b) **FS**

Figure 14: **Uilenspiegel**:**WIP** Scale influence on the isowakes at station 2

4.2.5 Comparisons with full scale experiments

Once the full scale free-surface computations were completed, the full-scale experiments carried out by the EFFORT consortium were comunicated. Consequently, this section is devoted to a comparison of ISIS-CFD computations with the experimental isowake distribution at two different sections for "Windows A & C" and "Windows D & E" which will not be explictly specified for confidentiality reasons.
Figure 16 shows a comparison between the experiments and the blind computations performed in the same conditions (full scale free-surface flow with an operating propeller) at

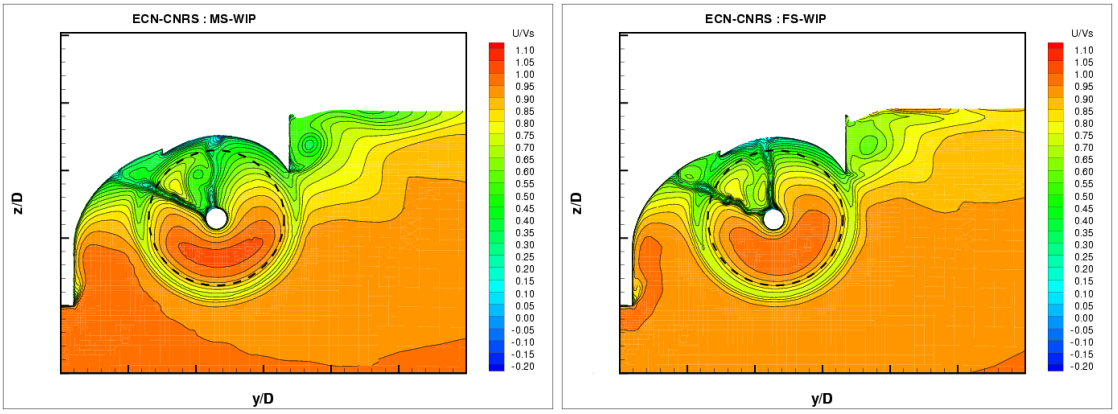

(a) **MS** (b) **FS**

Figure 15: **Uilenspiegel**:**WIP** Scale influence on the isowakes at station 3

windows A and C. The agreement between these two results is excellent and very reassuring with respect to the predictive capabilities of ISIS-CFD associated with the HEXPRESS grid generation tool. The distorted region of low velocity corresponding to the wake of the propeller shaft and boss is very well captured by the numerical simulations which were done with the $k-\omega$ SST model.

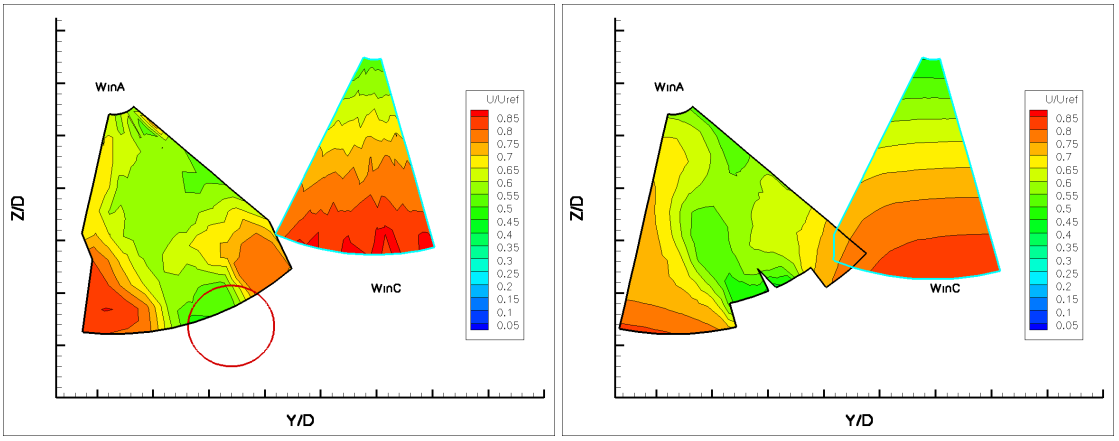

(a) Full scale experiments (b) Full scale SST computations

Figure 16: **Uilenspiegel**:**WIP**:WinAC: Comparison on the isowake distribution between full scale experiments and ISIS-CFD computations at windows A and C

Lastly, Figures 17 show a comparison between the full scale experiments and the computations at windows D and E. Once again, from the isowake distribution comparison, one can observe that the agreement between experiments and blind computations is excellent.

5 CONCLUSIONS

Appended hull configurations are investigated in the present study. The use of hexahedral unstructured grid generator HEXPRESS allows to maintain the accuracy of the finite-volume flow solver and to reduce the mesh generation time from weeks to a few days compared to block-structured grid generator. Due to the inherent default of the unstructured grid generator, numerical solution may not be as accurate as that obtained with

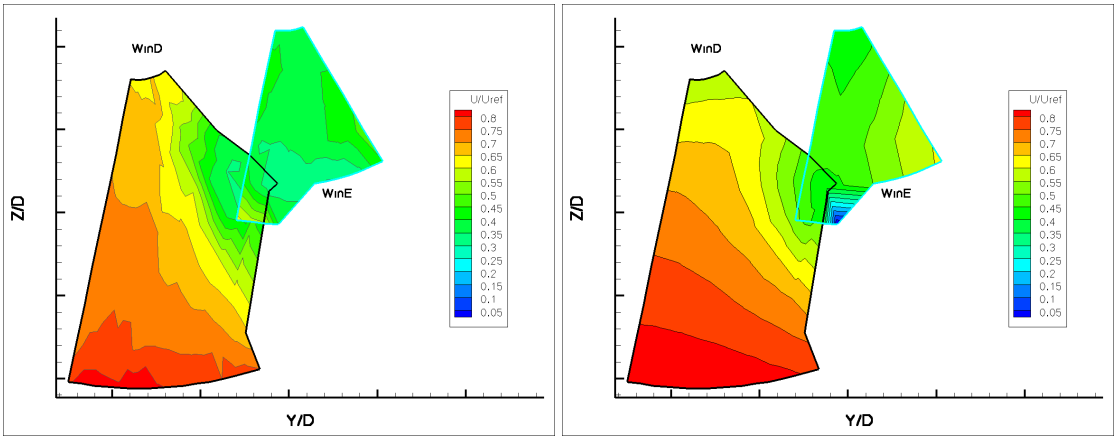

(a) Full scale experiments (b) Full scale SST computations

Figure 17: **Uilenspiegel**:**WIP**:WinDE: Comparison on the isowake distribution between full scale experiments and ISIS-CFD computations at windows D and E

a structured mesh. However, discretization error is expected to be smaller than a few percents when grid is fine enough. As expected, flow with appendages becomes more challenging for numerical simulation. The longitudinal vortex generated from the sonar bulb for example, makes the accurate prediction of the boundary layer along the hull difficult. The validation of the wall function approach becomes questionable. The successful prediction obtained in the present study contains advanced features in turbulence modelization such as nonlinear model and rotation correction implemented in our ISIS-CFD code. In addition, low Reynolds number model has to be used in order to obtain a reliable prediction. Such an approach is quite different from usual practice in engineering applications based on commercial software. The performance of the ISIS-CFD code is also demonstrated in a computation at model and full scale for a fully appended hull configuration including free-surface, ducted propeller, brackets and rudder. The agreement between the blind computations and the full scale experiments is very satisfactory and seems to indicate that CFD tools may be used with confidence for the design of complex ship hulls in full scale conditions. A complete analysis of the scale effects on free-surface and of the structure of the viscous stern flow reveals that these scale effects are not negligible and depend strongly on the stern geometries.

6 ACKNOWLEDGMENTS

This work was supported by the European EFFORT project No. GRD2-2001-50117. The authors are indebted to Mr. Erwan Jacquin of Bassin d'Essais des Carènes for providing us with the experimental data for the frigate "Commandant Rivière".

REFERENCES

[1] P. R. Spalart and S. R. Allmaras, "A one-equation turbulence model for aerodynamic flows." AIAA Paper 92-0439, 1991. 2

[2] F. Menter, "Zonal two-equations $k-\omega$ turbulence models for aerodynamic flows.," *AIAA Paper*, vol. 93-2906, 1993. 2

[3] G. Deng, P. Queutey, and M. Visonneau, "Three-dimensional flow computation with reynolds stress and algebraic stress models," *Engineering Turbulence Modeling and Experiments 6*, vol. 6, pp. 389–398, 2005. 2

[4] R. Duvigneau, M. Visonneau, and G. Deng, "On the role played by turbulence closures for hull shape optimization at model and full scale," *Journal of Marine Science and Technology*, vol. 8, June 2003. 2

[5] B. d'Essai des Carènes, "Ldv data concerning the cdt. riviere," tech. rep., Internal report, Val de Reuil, 1999. 2

[6] F. Stern, R. Wilson, H. Coleman, and E. Paterson, "Verification and validation of cfd simulations," Tech. Rep. 407, IIHR Report, 1999. 4, 6

[7] G. Deng, E. Guilmineau, P. Queutey, and M. Visonneau, "Ship flow simulations with the isis-cfd code," in *CFD WORKSHOP TOKYO 2005* (T. Hino, ed.), Tokyo, Japan, pp. 474–482, 2005. 4, 7

[8] G. Deng and M. Visonneau, "On the prediction of swirling induced recirculation," in *3rd Int. Sym. on Turbulence and Shear Flow Phenomena*, Sendai,Japan, 2003. 6

[9] L. Eça and M. Hoekstra, "An uncertainty estimation exercise with the finite-difference and finite-volume versions of parnassos," in *Workshop on CFD Uncertainty Analysis* (L. Eça and M. Hoekstra, eds.), Lisbon, Portugal, 2004. 6